JBC RESEARCH ARTICLE

Distinct conformers of amyloid beta accumulate in the neocortex of patients with rapidly progressive Alzheimer's disease

Received for publication, May 11, 2021, and in revised form, September 27, 2021 Published, Papers in Press, September 30, 2021,
https://doi.org/10.1016/j.jbc.2021.101267

He Liu[1], Chae Kim[1], Tracy Haldiman[1], Christina J. Sigurdson[2,3], Sofie Nyström[4], K. Peter R. Nilsson[4], Mark L. Cohen[1,5], Thomas Wisniewski[6,7], Per Hammarström[4], and Jiri G. Safar[1,8,*]

From the [1]Department of Pathology, Case Western Reserve University, Cleveland, Ohio, USA; [2]Department of Pathology and [3]Department of Medicine, University of California, San Diego, La Jolla, California, USA; [4]Department of Physics, Chemistry, and Biology, Linköping University, Linköping, Sweden; [5]National Prion Disease Pathology Surveillance Center, Case Western Reserve University, Cleveland, Ohio, USA; [6]Centre for Cognitive Neurology, Department of Neurology, New York University School of Medicine, New York, New York, USA; [7]Department of Psychiatry, New York University School of Medicine, New York, New York, USA; [8]Department of Neurology, Case Western Reserve University, Cleveland, Ohio, USA

Edited by Paul Fraser

Amyloid beta (Aβ) deposition in the neocortex is a major hallmark of Alzheimer's disease (AD), but the extent of deposition does not readily explain phenotypic diversity and rate of disease progression. The prion strain–like model of disease heterogeneity suggests the existence of different conformers of Aβ. We explored this paradigm using conformation-dependent immunoassay (CDI) for Aβ and conformation-sensitive luminescent conjugated oligothiophenes (LCOs) in AD cases with variable progression rates. Mapping the Aβ conformations in the frontal, occipital, and temporal regions in 20 AD patients with CDI revealed extensive interindividual and anatomical diversity in the structural organization of Aβ with the most significant differences in the temporal cortex of rapidly progressive AD. The fluorescence emission spectra collected *in situ* from Aβ plaques in the same regions demonstrated considerable diversity of spectral characteristics of two LCOs—quatroformylthiophene acetic acid and heptaformylthiophene acetic acid. Heptaformylthiophene acetic acid detected a wider range of Aβ deposits, and both LCOs revealed distinct spectral attributes of diffuse and cored plaques in the temporal cortex of rapidly and slowly progressive AD and less frequent and discernible differences in the frontal and occipital cortex. These and CDI findings indicate a major conformational diversity of Aβ accumulating in the neocortex, with the most notable differences in temporal cortex of cases with shorter disease duration, and implicate distinct Aβ conformers (strains) in the rapid progression of AD.

The hallmark of sporadic Alzheimer's disease (sAD) is the accumulation of misfolded aggregates of amyloid beta (Aβ) and hyperphosphorylated tau forming neurofibrillary tangles (NFTs) (1). AD encompasses remarkably variable phenotypes and progression rates, classified by the dominant clinical symptomatology as an amnestic variant, posterior cortical atrophy, logopenic primary progressive aphasia, and the frontal variant of AD. Moreover, based on the neuroimaging and neuropathology data, these clinical phenotypes have been divided into typical AD, with balanced NFT counts in the hippocampus and association cortex; limbic-predominant AD, with counts predominantly in hippocampus; and hippocampal-sparing AD, with counts predominantly in the association cortex (2, 3). The sources of this clinicopathological heterogeneity are not understood, and current data on genetic polymorphisms can explain only ∼30% of the variability (4–7).

The AD pathology is characterized as a dual proteinopathy, and one of its pivotal criteria for establishing standardized neuropathologic diagnosis of AD is the accumulation of misfolded Aβ forming plaques, especially those with dense-core and diffuse morphotypes (8–10). Growing evidence from transgenic and cell transmission experiments suggests a prion-like propagation of protein misfolding, implying the role of differently misfolded structures in distinct phenotypes of neurodegeneration (11–16). Our early work established a linkage between distinct Aβ42 (human amyloid beta peptide with amino acid sequence 1 to 42) conformers and rapidly progressive AD (rpAD) at a biophysical level, by utilizing advanced conformation-sensitive immunoassays originally developed for differentiation of prion strains (12, 17–21). The different Aβ structures in distinct AD phenotypes we found with conformation-dependent immunoassay (CDI) and conformational stability assay were subsequently confirmed by the solid-state NMR (ssNMR) of Aβ replicated from the brain tissue of patients with rpAD (22) and by X-ray microdiffraction study in tissue sections derived from patients with AD (23). More recently, the cryo-EM has shown that conformations of brain-derived Aβ amyloid fibrils are heterogeneous, and distinctly different structures from Aβ fibrils are formed *in vitro* (24). However, these structural methods required a templated conversion or complex purification procedure that may distort structural characteristics that exist *in vivo*.

* For correspondence: Jiri G. Safar, jiri.safar@case.edu,

Recently, synthesized luminescent conjugated oligothiophenes (LCOs) are ultrasensitive fluorescence dyes that allow the monitoring of different amyloid structures directly in the intact frozen brain tissue (25–32). The growing family of these ligands demonstrated a high affinity for misfolded protein aggregates harboring repetitive cross β-sheet amyloid structure and considerable conformational sensitivity sufficient to differentiate structurally distinct prion strains in rodents (33–35) and thus fulfill the criteria sought for new amyloid probes (36). Here, we compared the fluorescence spectral analysis of two chemically different LCOs upon binding to Aβ plaque morphotypes in three anatomical regions of rpAD and slowly progressive AD (spAD) cases and then correlated the data with CDI and immunohistochemistry using conformation-sensitive antibodies. The results demonstrated extensive molecular landscape for distinct conformers of Aβ in diverse clinical phenotypes and major interindividual variability in Aβ structural organization. The LCOs were able to corroborate this conclusion in different plaque morphotypes formed by Aβ with different conformations directly *in situ* in the brain cortex sections of patients with AD.

Results

Comparative demographics and neuropathology in rpAD and spAD

The rapidly progressive cases of AD were initially referred to the National Prion Disease Pathology Surveillance Center (NPDPSC) as rapidly progressive or atypical dementia with working diagnosis of probable prion diseases, but these cases subsequently failed to confirm neuropathologic or genetic evidence for prion disease after prion protein (PRNP) gene sequencing and instead established definite neuropathological diagnosis of AD according to the National Institutes of Aging—Alzheimer's Association (NIA-AA) (5) (Table 1). From 186 cases with an identifiable disease starting date which we obtained from detailed clinical records and semistructured telephone interviews with patients and/or caregivers at the time of referral, we selected 32 cases with the available frozen frontal, occipital, and temporal cortex (17, 37, 38). Our second cohort consisted of 34 classical AD cases collected at New York University (NYU) Alzheimer Disease Center (see the Experimental procedures section) that matched our previously reported Case Western Reserve University cohort (17, 37) and progression rates and demographics distribution in the National Alzheimer's Coordinating Center dataset and hereafter was referred to as spAD (Fig. 1, *A* and *B* and Table 1) (17, 37, 38). The faster progression in rpAD cases was associated with younger age at death, which agreed with findings from our previous studies (17, 37, 38) and with data from prion centers in Japan and Europe (39). Neuropathological evaluation according to the NIA-AA guidelines (5, 17) indicated a higher variance and trend toward more cases with less severe Aβ deposition in the rpAD group; the differences in other criteria including the pathology of tau using AT8 immunohistochemistry were not statistically significant (Fig. 1*C* and Table 1). In addition, diffuse Aβ and intracellular Aβ deposits

Table 1
Demographics, clinicopathological characteristics, levels, and conformation of Aβ42 in the neocortex of AD cases with malignant rapidly progressive and classical slowly progressive disease phenotype

Parameter		Unit	rpAD				Significance	spAD			
			n	Minimum	Maximum	Mean ± SEM	*p*	n	Minimum	Maximum	Mean ± SEM
Sex		Female/male	15/17				NS	19/15			
Age		Years	32	54	87	67.2 ± 1.6	<0.001	34	61	101	79.6 ± 1.8
Disease duration	From neurological follow-up	Month	30	0.8	39	14.3 ± 2.1	<0.001	31	36	300	110.6 ± 10.0
PMI		h	32	2	120	41.6 ± 5.4		31	4	42	15.8 ± 1.6
ApoE	*e2*	n (%)	1 (2.1)					3 (4.4)			
	e3	n (%)	33 (68.8)				0.003	35 (51.5)			
	e4	n (%)	14 (29.2)					30 (44.1)			
Neuropathological classification	A	Range	30	1	3	2.17 ± 0.18	0.003	33	1	3	2.79 ± 0.08
	B	Range	30	1	3	2.57 ± 0.15	NS	33	1	3	2.88 ± 0.07
	C	Range	30	1	3	2.07 ± 0.20	NS	33	1	3	2.36 ± 0.14
Aβ42	Frontal	ng/ml	9	304.1	503.9	384.9 ± 23.4	NS	11	118.5	619.3	324.3 ± 36.7
		D/N ratio	9	14.1	37.8	20.4 ± 2.4	NS	11	8.2	30.1	16.0 ± 2.2
	Occipital	ng/ml	9	6.3	524.4	282.6 ± 55.2	NS	11	16.1	667.8	321.6 ± 54.8
		D/N ratio	9	0.9	33.5	15.3 ± 2.9	NS	11	1.5	27.5	16.2 ± 2.7
	Temporal	ng/ml	9	10.3	507.5	284.7 ± 55.3	NS	18	223.7	498.2	332.5 ± 19.8
		D/N ratio	9	0.9	28.5	18.1 ± 2.8	0.022	18	9.9	33.3	24.4 ± 1.3

Abbreviation: NS, not significant.

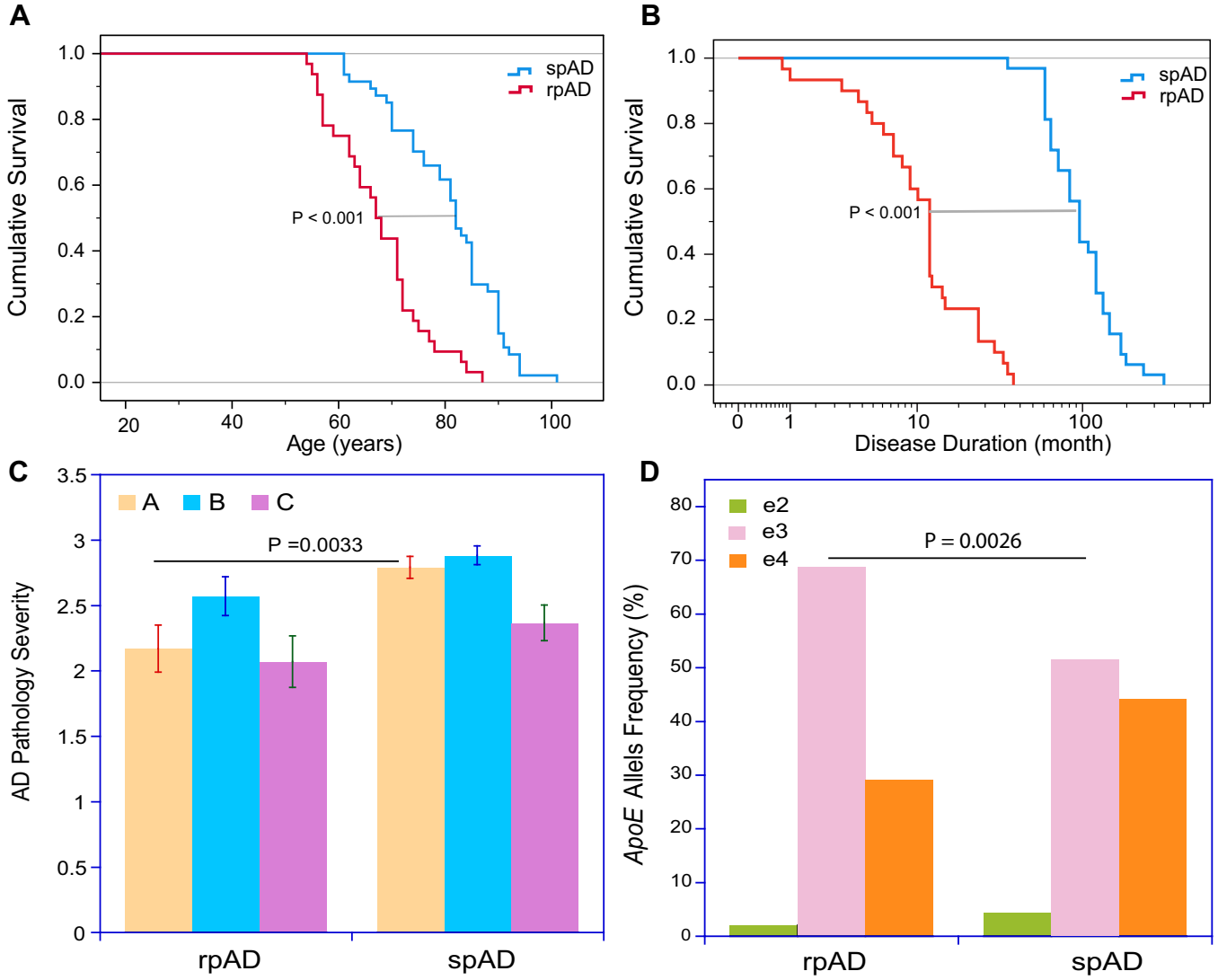

Figure 1. Cumulative survival, progression rates, *APOE* gene allelic frequency, and neuropathology profiles of Alzheimer's disease (AD) cases. *A,* Kaplan–Meier cumulative survival analysis and (*B*) duration of disease of cases with pathologically verified AD that were initially referred to National Prion Disease Pathology Surveillance Center with rapidly progressive dementia (rapidly progressive AD [rpAD], n = 32) and cases of slowly progressive AD (spAD, n = 34) collected at New York University Alzheimer Research Center (17). Statistical significance for difference in survival at $p < 0.001$ (***) was determined with the log rank (Mantel–Cox test). *C,* severity of pathology classified according to National Institute on Aging–Alzheimer's Association guidelines for the neuropathologic assessment in rpAD and spAD: "A" indicates phase assessment of the Aβ deposits severity; "B" is staging neurofibrillary tau pathology; and "C" (CERAD) is scoring the extent of Aβ plaques (73). *D,* frequency of e3 allele of *APOE* gene allelic polymorphisms in rapidly and slowly progressive cases of AD. Statistical significance was determined with two-tailed Fisher's exact test.

in microglia and astrocytes (40) occurred inconsistently in both rpAD and spAD cases, and if present, constituted a minor fraction of the total Aβ deposition (17). Finally, as reported earlier by us and others (17, 22), the amyloid plaque morphotypes and the deposits of hyperphosphorylated tau in all three cortex areas did not differ significantly between rpAD and spAD cases, and there were no pattern differences between rpAD cases with variable disease duration (Fig. 1*C* and Table 1). The NYU cohort of spAD showed significantly higher frequency of *e4 APOE* (apolipoprotein E gene with ε2, ε3, or ε4 allelic polymorphisms) alleles as previously with Case Western Reserve University cases (17) (Fig. 1*D* and Table 1). Cumulatively, the consistent rapid progression rate and neuropathological findings of rpAD in prion and Alzheimer's centers across various methodologies, populations, and health care systems is evidence for a distinct and especially malignant form of sAD (11, 17, 37, 39, 41–43).

Distribution and conformation of Aβ42 in neocortex of rpAD and spAD

To investigate levels and conformational characteristics of Aβ, we adopted an AlphaLISA-formatted CDI (12, 18, 19, 21). This extremely sensitive assay played a critical role in discovering that a variable proportion of pathogenic prion protein is composed of small protease-sensitive oligomers and also helped to establish that the conformation of pathogenic prion protein varies between distinct strains of prions (12, 18, 19, 21).

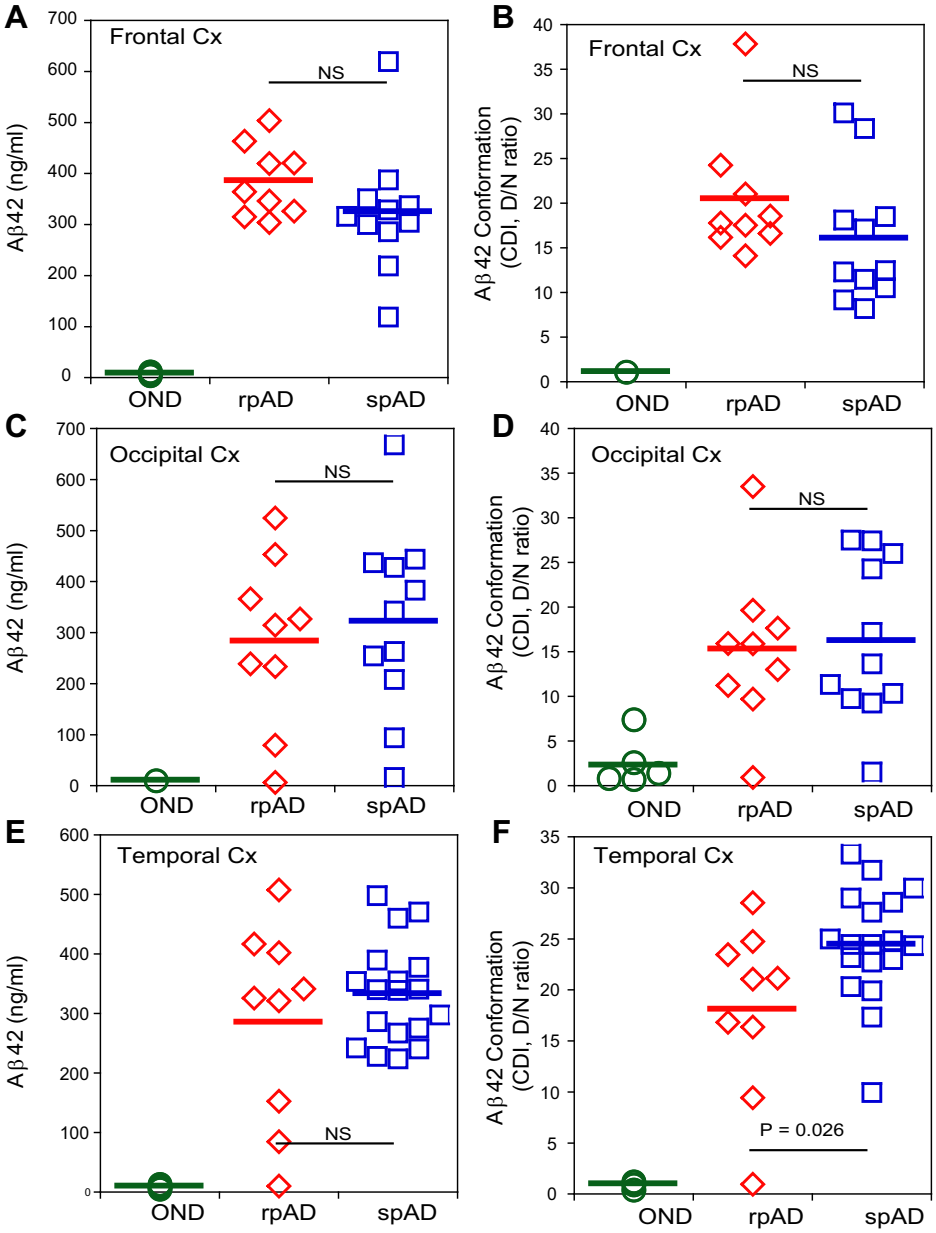

Figure 2. Conformational profiles and levels of amyloid beta (Aβ42) in the frontal, occipital, and temporal neocortex of Alzheimer's disease (AD) patients and non-AD controls. Concentration (*left panels*) and conformational profile (*right panels*) of Aβ42 in (*A* and *B*) frontal cortex, (*C* and *D*) occipital cortex, and (*E* and *F*) temporal cortex of rapidly progressive AD (rpAD) (*red*) and slowly progressive AD (spAD) (*blue*) cases were investigated. The data were obtained with alphaLISA-formatted conformation-dependent immunoassay before (native, N) and after complete denaturation with guanidine hydrochloride (denatured, D) (17). The concentrations are expressed in nanograms per milliliter of 10% brain homogenate, and different D/N ratios indicate the presence of varying Aβ42 conformations. Each data point here represents an average of two measurements for the given anatomical region of each individual case. The statistical significance was determined with two-way ANOVA. NS, not significant; OND (*green*), other neurodegenerative diseases.

In principle, we adopted the AlphaLISA design with one antibody specific to the N terminus (monoclonal antibody [mAb] 4G8; epitope Aβ17-24) and a second antibody specific either to the C terminus of Aβ42 (mAb12F4) or Aβ40 (human amyloid beta peptide with amino acid sequence 1 to 40; mAb 11A50-B10) (17). The luminescence signal is generated only when the donor and acceptor beads are brought together in close proximity by simultaneous capture of N and C terminus of Aβ (17). Measurements performed before and after denaturation with 7 M guanidine hydrochloride (GdnHCl) at 80 °C, expressed as a denatured/native (D/N) signal, allow quantitation of the exposure of both domains in the native state, thereby enabling direct comparison of global assembly structures in different brain samples without requiring prior purification (16, 19, 21, 44–46).

Our recent CDI study showed comparable high concentrations of Aβ42 accompanied by consistently low levels of Aβ40 in posterior cingulate and hippocampus cortex of rpAD and spAD cases (17). Here, we expanded these data to frontal, occipital, and temporal cortex (Fig. 2, *A*, *C*, and *E*), and as

previously, the concentrations of Aβ42 were comparable in rpAD and spAD cases in all anatomical areas. Similarly, the low levels and consistently low conformational D/N ratio of Aβ42 in non-AD controls indicate that both N and C termini are largely exposed in the native state (Fig. 2, *B*, *D*, and *F*) in an open conformation of monomers (17). In contrast, we observed a broad data variation of high D/N ratios in all neocortex areas of AD cases, with significantly lower median values in the temporal cortex of rpAD cases. Taken together, these data indicate that although Aβ42 accumulates in both the temporal cortex of rpAD and spAD cases at approximately the same levels, the Aβ42 found in rpAD forms either (i) smaller particles, (ii) particles with a differently exposed N and C termini of Aβ42 because of the distinct conformation, or (iii) both. The data presented here and obtained previously in age-matched non-AD controls including sporadic Creutzfeldt–Jakob disease indicate that these aspects are not a simple result of aging (17).

Colabeling of amyloid plaques with quatroformylthiophene acetic acid and heptaformylthiophene acetic acid LCOs

To ascertain the global amyloid plaque load and characteristics in different neuroanatomical regions, we performed fluorescence spectroscopy in randomly selected rpAD and spAD cases with a rapid colabeling protocol using mixture of quatroformylthiophene acetic acid (qFTAA) and heptaformylthiophene acetic acid (hFTAA) LCOs (Fig. 3, *A* and *B*). The fluorescent images and emission spectra were collected from cryosections obtained from the frontal, occipital, and temporal cortex in a large number of plaques with the long pass emission filter in the range of 480 to 700 nm (Fig. 3*C*). In

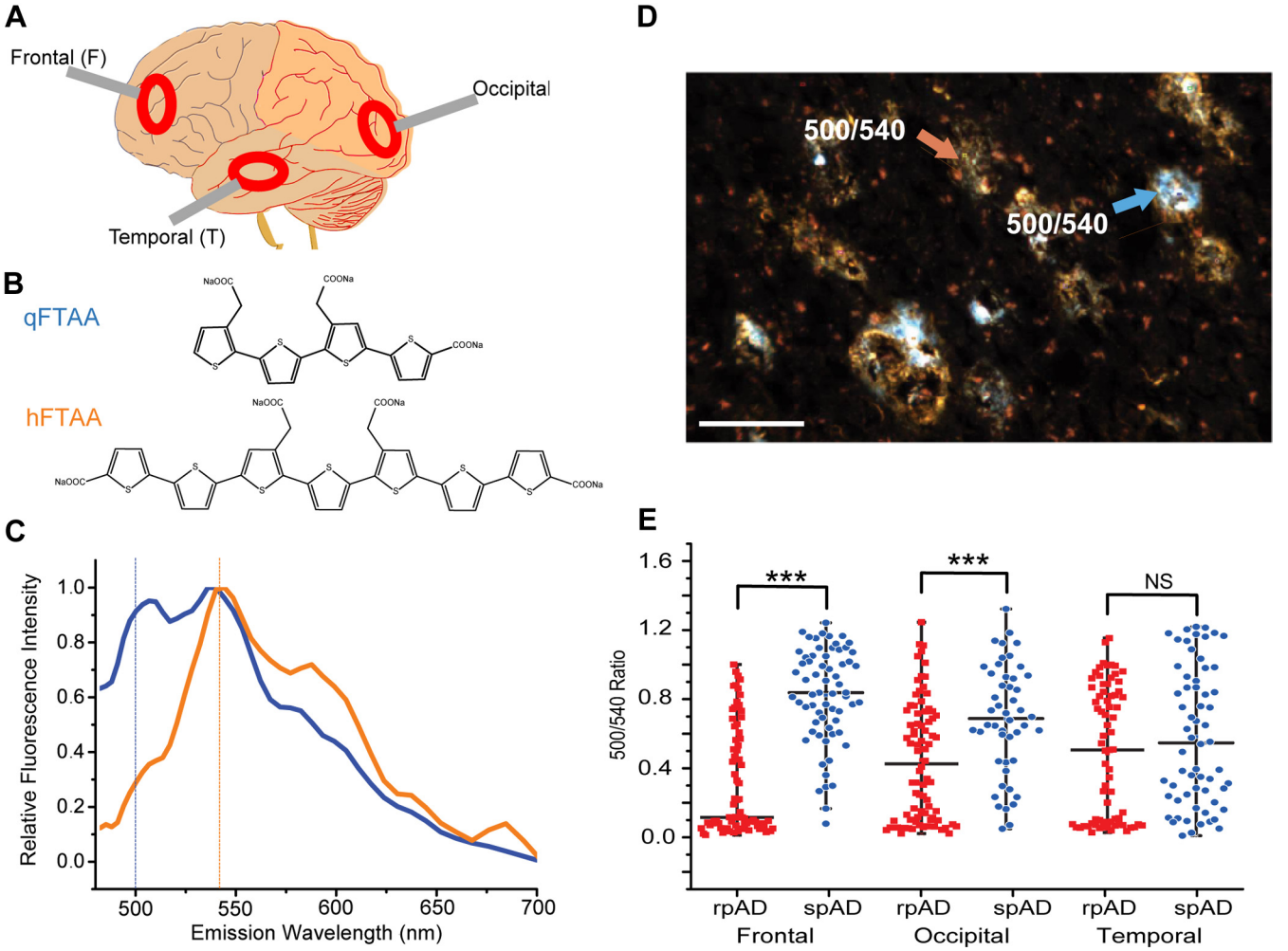

Figure 3. Differential labeling of amyloid plaques in Alzheimer's brain neocortex with conformation-sensitive luminescent conjugated oligothiophenes (LCOs). Differential characteristics of amyloid plaques in frontal (F), occipital (O), and temporal (T) neocortex (*A*) of rapidly progressive Alzheimer's disease (rpAD) and slowly progressive Alzheimer's disease (spAD) patients were investigated by colabeling with two chemically different LCOs —qFTAA and hFTAA. *B,* The fluorescence emission spectrum of qFTAA is shown in *blue*, whereas that of hFTAA is represented in *orange*. Distinct emission spectra of qFTAA and hFTAA in a typical Aβ plaque; contribution of qFTAA and hFTAA binding to plaques was evaluated at 500 nm (qFTAA) and 540 nm (hFTAA) after excitation at 436 nm, respectively. *C, orange areas* in dual labeling indicate binding of hFTAA but not qFTAA to the plaques, whereas *blue and white areas* are depicting binding of both dyes. *D,* the scale bars represent 100 μm. Ratio of fluorescence intensity at 500/540 was measured in the frontal, occipital, and temporal cortex plaques (n) (*red squares*, n = 74, 80, and 73, respectively) of rpAD, and in frontal, occipital, and temporal cortex plaques (n) (*blue circles*, n = 65, 48, and 62, respectively) of spAD. Each ratio data point represents one plaque. *E,* NS; ***$p < 0.005$. hFTAA, heptaformylthiophene acetic acid; NS, not significant; qFTAA, quatroformylthiophene acetic acid.

this protocol, Aβ deposits represented in *orange* indicate preferential binding of hFTAA but not qFTAA, whereas these in *blue* and *white* represent binding of both qFTAA and hFTAA (Fig. 3*D*). The ratio of characteristic qFTAA and hFTAA peak maxima at 500 and 540 nm (*dashed lines*) indicated distinct Aβ patterns in different plaques (Fig. 3*C*). The higher ratio is consistent with the preferential binding of qFTAA to compact plaques, whereas the diffuse plaques accumulating Aβ with preferential binding of hFTAA had lower ratio (Fig. 3, *C* and *D*). The comparison of rpAD and spAD revealed major differences in LCO staining patterns between patients with rpAD and spAD in the frontal and occipital regions but not in the temporal region (Fig. 3*E*). In contrast to the normal distribution of data in spAD cases, the data in all anatomical areas of rpAD cases indicated skewed distribution and large kurtosis separating the fluorescence emission attributes into two apparent subsets, and similar trend appears in the temporal area of spAD cases. Cumulatively, the double labeling protocol points to a significant difference in plaque-forming Aβ populations between rpAD and spAD and at least two distinct conformer sets of Aβ in all anatomical areas of rpAD cases. In addition, the double LCO labeling indicates abundance of mature cored plaques with high 500/540 ratio in temporal and occipital areas and a lower frequency of plaques with these spectral attributes in the frontal lobe of rpAD cases; an opposite trend was observed in spAD (Fig. 3*E*).

Diversity of Aβ amyloid deposits labeled with qFTAA, hFTAA, and conformation-sensitive antibody

To investigate whether the differences between rpAD and spAD cases could be due to the distinct spectral attributes of different plaques or differential binding affinity of qFTAA and hFTAA, we performed separate labeling with each LCO and separate evaluation of plaques with distinctly different morphologies: highly dense-cored and diffuse Aβ plaques and data correlated with immunohistochemistry (Fig. S1). The conformation-sensitive OC antibody detects Aβ amyloid deposits composed of subsets of Aβ amyloid fibrils and Aβ oligomers. In both cored and diffuse plaques, hFTAA staining overlapped more frequently with OC-antibody positive plaque areas. In contrast, qFTAA detected preferentially compact plaque areas, which was consistent with our observation from a double labeling protocol (Fig. 3*D*). Notably, OC-positive Aβ deposits were distributed sparsely around qFTAA-positive plaques, whereas they were overlapping with amyloid deposits decorated with hFTAA and in cerebral amyloid angiopathy (Fig. S1). Conversely, the qFTAA shows minimal or no overlap with OC-positive Aβ deposits in cerebral amyloid angiopathy. Based on these data, we argue that qFTAA and hFTAA have distinctly different affinities for Aβ plaque substructures with different morphologies. The similarity and overlapping staining of hFTAA with OC antibody suggests binding to similar conformers of Aβ including oligomers and/or unique fibrillar Aβ subset. Cumulatively, hFTAA shows sensitivity to a wider spectrum of Aβ deposits including compact and diffuse plaques than qFTAA.

Comparative analysis of spectral attributes of Aβ conformers labeled with qFTAA in cored and diffuse plaques of rpAD and spAD cases

Because of the apparent difference in affinities of LCOs to different amyloid deposits (Fig. 3), we performed first the staining of cored and diffuse plaques in frontal, occipital, and temporal regions of rpAD and spAD cases with qFTAA. The normalized averaged spectra recorded from 470 to 690 nm with 10 nm bandwidth allowed us to collect emission spectra from cored plaques and diffuse plaques. The averaged spectra showed major differences between the qFTAA signature of cored (Fig. 4, *A*–*C*) and diffuse plaques (Fig. 4, *D*–*F*) recorded in all anatomical regions of patients with rpAD and spAD. To evaluate quantitatively interindividual distribution of spectral signatures of Aβ plaques stained by qFTAA, we used two characteristic data points at 500 and 510 nm as a ratio. Even with an extensive variability of the qFTAA 500/510 nm ratios, the data indicate significant differences in cored plaques in the frontal ($p < 0.001$) and temporal regions ($p < 0.01$) of rpAD and spAD cases but not in the occipital cortex (Fig. 4*G*). The signatures of diffuse plaques showed the same trends, and the differences in occipital cortex became statistically significant ($p < 0.001$) (Fig. 4*H*). Taken together, the distinct qFTAA spectral signatures suggest that Aβ-forming compact and diffuse plaques have different conformations. The extensive interplaque and interindividual variability is a direct *in situ* evidence of the structural diversity of Aβ accumulating in compact and diffuse plaques present in rapid and slowly progressing AD cases.

Spectral attributes of Aβ conformers detected with hFTAA in cored and diffuse plaques of rpAD and spAD cases

Adjacent frozen sections stained with qFTAA were subsequently stained with hFTAA, and the spectra of cored (Fig. 5) and diffuse plaques (Fig. 6) were collected for rpAD and spAD cases in three different anatomical regions. The emission spectrum of hFTAA bound to Aβ is more complex, and therefore, we selected four characteristic fluorescence ratios: 550/510, 580/510, 550/500, and 580/500 nm. Herein, 500 or 510 nm, where hFTAA emission is low, is used as an internal reference of amyloid autofluorescence (47). In cored plaques, ratios differed significantly and discriminated rpAD from spAD cases in all three brain regions. Notably, the 550/500 ratio readily distinguished rpAD from spAD cases in all three regions with a high reliability (all $p < 0.001$) (Fig. 5*G*), and similar trends were observed for the 550/510 nm ratio (Fig. 5*F*). The 580/500 nm (Fig. 5*E*) and 580/510 nm (Fig. 5*D*) ratios confirmed these observations with a different statistical significance. The findings indicate that spectral attributes of hFTAA discriminate cored Aβ plaques present in different brain areas of these two different AD phenotypes. As per diffuse plaques (Fig. 5, *A*–*C*), all selected ratios uniformly showed highly significant differences in the temporal region

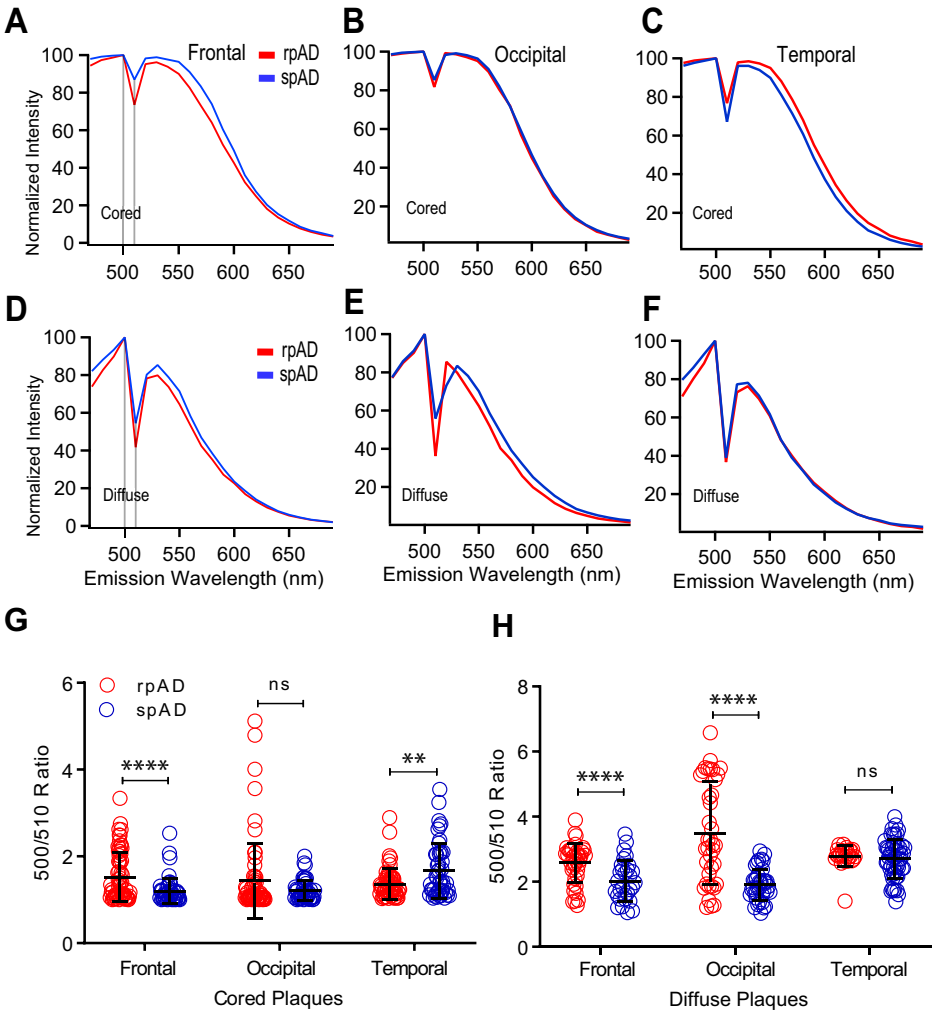

Figure 4. Fluorescence spectra analysis of Aβ in cored and diffuse plaques labeled with qFTAA in different neocortex regions of rpAD and spAD cases. Mean emission spectra profiles of cored (*A–C*) and diffuse (*D–F*) plaques in the frontal, occipital, and temporal cortex of five rpAD (*red*) and 11 spAD (*blue*) randomly selected cases were labeled by qFTAA and recorded from 470 to 690 nm and expressed as a fluorescence intensity ratio of 500 to 510 nm (500/510 ratio) for compact (G) and diffuse (H) plaques, as described in the Experimental procedures section and Table S1. Each ratio data point represents one plaque; the full emission spectra of cored and diffuse plaques were recorded for each plaque in ten different spots, averaged, and normalized; bars indicate mean ± SD; ns; $^{**}p < 0.01$, $^{****}p < 0.001$. ns, not significant; qFTAA, quatroformylthiophene acetic acid; rpAD, rapidly progressive Alzheimer's disease; spAD, slowly progressive Alzheimer's disease.

($p < 0.001$) (exception for 580/500 ratio: $p < 0.005$) but not in the frontal and occipital regions (Fig. 6, *D–G*). Cumulatively, the data indicate an extensive heterogeneity of Aβ present in diffuse and compact plaques. The high conformational sensitivity of hFTAA revealed the existence of distinct Aβ conformers in diffuse plaques in the temporal region of rpAD and spAD cases and could be used as a potential diagnostic tool.

The CDI conformational data (D/N ratios) obtained with AlphaLISA in the total cortex homogenates represent cumulative signal of oligomers and mixture of different plaques (17) and show significant differences in the Aβ42 conformation in temporal cortex. The data confirm that the differences found in this area for compact plaques stained with qFTAA (Fig. 4) and for both cored and diffuse plaques stained with hFTAA (Figs. 5 and 6). Cumulatively, the AlphaLISA and fluorescence emission spectra patterns of both LCOs indicate major differences in the conformation of Aβ in the temporal cortex, with additional differences detected less frequently in the frontal and occipital cortex (Table S2, *A* and *B*).

3D landscape of conformational characteristic of Aβ42 in diffuse plaques detected with hFTAA in the temporal regions of rpAD and spAD cases, age, and disease duration

To summarize the spectral differences obtained from the different brain regions, we constructed a heat map based on statistical differences (Table S2). The heat map shows that hFTAA fluorescence attributes of diffuse plaques in the temporal cortex and compact (cored) plaques in the frontal cortex clearly separate rpAD from spAD (Table S2*A*). Fluorescence emission spectra of qFTAA differentiate cored and diffuse plaques in the frontal cortex and diffuse plaques in the occipital cortex of rpAD and spAD cases (Table S2*B*). To investigate the spectral attributes of diffuse plaques stained

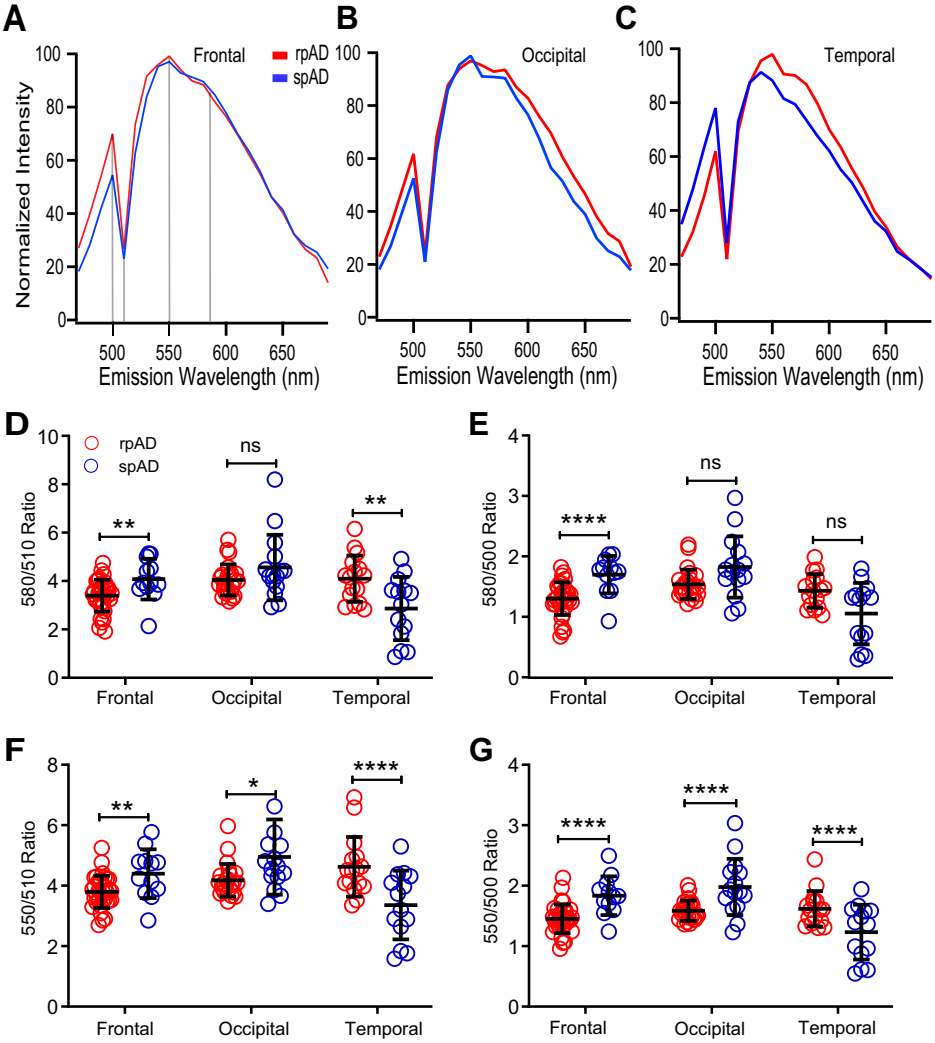

Figure 5. Fluorescence spectra analysis of Aβ in cored plaques labeled with hFTAA in different regions of rpAD and spAD cases. Normalized mean emission spectra of cored plaques in frontal (*A*), occipital (*B*), and temporal (*C*) neocortex of five cases with rpAD (*red*) and 11 cases with spAD (*blue*) labeled by hFTAA and recorded from 470 to 690 nm as described in the Experimental procedures section and Table S1. Normalized spectral attributes are expressed as wavelength ratio at 580/510 nm (*D*), 580/500 nm (*E*), 550/510 nm (*F*), and 550/500 nm (*G*). Each ratio data point in panel (*D–G*) represents one cored plaque recorded in ten different regions of interest, averaged, and normalized. Ratios in individual plaques are expressed as means ± SD; ns, not significant; $^{*}p < 0.05$, $^{**}p < 0.01$, $^{***}p < 0.005$, and $^{****}p < 0.001$. hFTAA, heptaformylthiophene acetic acid; ns, not significant; rpAD, rapidly progressive Alzheimer's disease; spAD, slowly progressive Alzheimer's disease.

with hFTAA in the temporal region of rpAD and spAD cases in relationship with the age and rate of the progression, we constructed a 3D landscape plot (Fig. 7). The data indicate that distinct Aβ conformations, here evidenced by hFTAA spectral ratio, correlate with a younger age of onset and shorter disease duration in rpAD and thus suggest clinicopathological criteria for an objective conformation-based classification of rpAD and spAD.

Discussion

The discrepancies between Aβ deposit levels and clinical disease severity (48) and the extensive variability of progression rates and phenotypes of AD (9) are two major phenotypic characteristics of late-onset AD that cannot be explained by genetic polymorphisms. We systematically analyzed different morphotypes of amyloid Aβ in neocortex of sporadic late-onset AD with an rpAD or an spAD progression of the disease utilizing two chemically different conformation-sensitive LCOs and correlated their spectral characteristics with the CDI and conformational antibodies. The extensive spectral LCO data on intact plaques recorded *in situ* and presented here provide strong evidence for the prion strain–like paradigm of different AD phenotypes, particularly the disease progression rate. These results and our previous longitudinal studies of ageing transgenic *APP* (amyloid precursor protein gene)/PS1 mice (49) potentially implicate differently folded Aβ conformers in accelerated reverse spread of pathology from temporal cortex to frontal cortex in rpAD, in contrast to propagation of amyloid deposits from neocortex to temporal region established in classical spAD.

Genetic evidence from familial AD (fAD) and genome-wide association studies of sporadic disease point to early

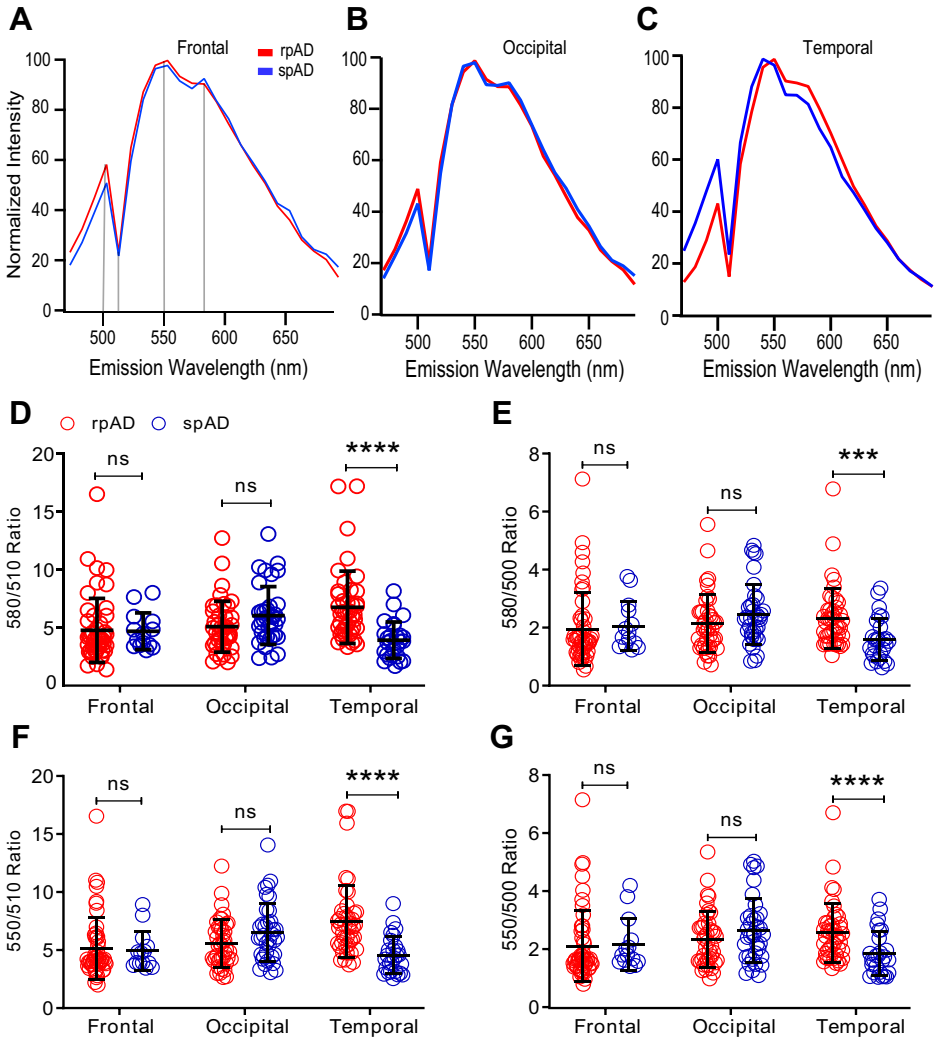

Figure 6. Comparative spectral analysis of Aβ in diffuse plaque morphotypes labeled with hFTAA in different regions of rpAD and spAD cases. Normalized mean fluorescence emission spectra of diffuse plaques in different regions of five rpAD (*red*) and 11 spAD (*blue*) cases labeled by hFTAA and recorded from 470 to 690 nm (*A–C*) as described in the Experimental procedures section and Table S1. *D–G,* normalized fluorescence intensity ratios for distinct peaks were evaluated. Each data point represents one diffuse plaque, full spectrum was recorded in 10 different regions of interest, averaged, and normalized. Emission wavelength ratios of individual plaques, each averaged from 10 recording spots, are expressed as means ± SD; ns; ***$p < 0.005$, ****$p < 0.001$. hFTAA, heptaformylthiophene acetic acid; ns, not significant; rpAD, rapidly progressive Alzheimer's disease; spAD, slowly progressive Alzheimer's disease.

imbalances of Aβ processing as a trigger for AD. However, there is also strong evidence that pathogenic forms of tau protein are an "executioner," giving rise to the main disease symptoms (50). Early seminal observations of transmissibility and acceleration of amyloid deposition in transgenic mice models with AD brain–derived amyloid (13, 32, 51) opened the possibility that alternatively structured amyloid can encipher the information essential for distinct phenotypes. Remarkably, recent studies point to the involvement of certain elements of prion-like mechanisms in AD. In particular, two of the most striking features of AD include (i) the discriminative anatomical targeting by which amyloid plaques and NFTs composed of hyperphosphorylated tau proteins spread through the brain (1, 50, 52) and (ii) the ability of toxic aggregates of Aβ and tau to serve as templates that convert their normal physiological precursors into new pathogenic forms by a prion-like mechanism (53). Moreover, our recent study with two distinct phenotypes of AD indicates that the AD brain Aβ exists in multiple structural states (prion-like strains) and that distinct conformers are associated with different progression rates and distinct disease symptomatology (17). Finally, fAD cases with PSEN1 mutations frequently have not only Aβ and tau protein deposit distribution and morphology different from spAD, but these deposits display a well-documented, yet unexplained, variability even within members of the same family (54–56). Based on these findings, along with transgenic bioassay data, and the fact that approximately 70% of phenotypic diversity in AD remains unexplained by polymorphisms in risk genes, we argue that structurally distinct prion-like strains of Aβ and tau aggregates may play a major role in the diverse pathogenesis of AD (16, 17, 57). However, despite the recent remarkable progress in high-resolution structural studies of Aβ amyloid fibrils and tau filaments by ssNMR (22, 58, 59) and cryo-EM (60, 61), the relationship between

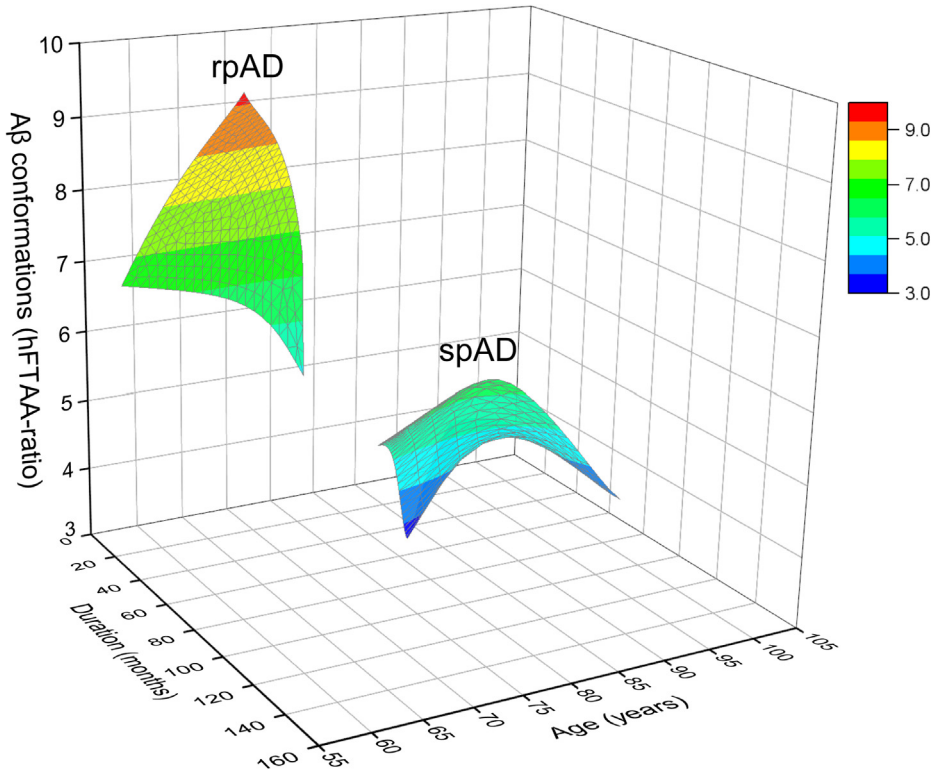

Figure 7. 3D correlations of conformational characteristics of Aβ in diffuse plaques in temporal cortex with the age and disease progression rate in rpAD and spAD cases. The 3D surface plot correlates age (years), duration of the disease (months), and conformational characteristic of Aβ (hFTAA ratio) in diffuse plaques present in the temporal cortex of individuals with rpAD (44 plaques in five cases) and spAD (27 plaques in six cases). The hFTAA ratio represents the averaged 550/510 ratio of diffuse plaques in the temporal region of each case; the different ranges of hFTAA ratios are indicated by the color scale. hFTAA, heptaformylthiophene acetic acid; rpAD, rapidly progressive Alzheimer's disease; spAD, slowly progressive Alzheimer's disease.

specific structural features of Aβ amyloid strains and phenotypic variability of AD remains largely unknown.

The conformation-sensitive LCOs have been utilized in recent years to study various misfolded proteins in human diseases and mouse models (35, 49, 62). The rationale for costaining amyloid plaques with qFTAA and hFTAA as described in previous studies (25, 27, 49) is the one step staining protocol, emission spectra collection, and evaluation. However, the resulting spectral attributes of staining with mixture of qFTAA and hFTAA are a complex outcome of a different affinity of each FTAA to a given amyloid conformer, differences in amyloid conformation, and possible fluorescence "crosstalk" (63). To improve our understanding of their behavior, we used each FTAA separately on an adjacent section. Based on our results, the previously reported higher 540/500 ratio of the mixture of qFTAA and hFTAA is consistent with the preferential binding of qFTAA to compact plaques, whereas the diffuse plaques accumulate Aβ with preferential binding of hFTAA and distinct emission spectra profiles. Cumulatively, the LCOs have distinct specificities: qFTAA binds preferentially to mature amyloid (cored plaques), whereas hFTAA detects immature amyloid deposits (diffuse plaques) as well as cored plaques.

The mechanistic aspects of distinct LCOs were extensively characterized by *in vitro* experiments with synthetic amyloid analogs (31, 32, 62). These and experiments with HET aggregates (26) suggest that LCO binds to a groove lined with repetitive positively charged side chains along the filament axis. This binding at 1.5 μM LCO concentrations is unlikely to induce a change in the amyloid conformation because the brain-derived Aβ42 is exceptionally stable; we did not observe a measurable unfolding up to 3 M GdnHCl (17). However, the degree to which the LCOs and oligomer-specific antibody binding may be modified by amyloid post-translational modifications will require a dedicated laser capture dissection and mass spectrometry of plaques (64, 65).

In this and our previous article (17) we observed with amyloid immunohistochemistry a less Aβ load in rapidly progressive cases (Fig. 1). Recent imaging mass spectrometry data showed that the diffuse amyloid aggregates in tgAPPSw mice model of AD are forming first, and that the maturation of these early deposits into cored plaques correlate with an apposition of Aβ40 (49, 65) and variable contribution of longer amyloid variants such as Aβ43 (66). Our data presented in this, and our earlier report, are consistent with these observations and implicate a distinct set of amyloid conformers in the faster disease progression and different rates of the plaque maturation. To determine a high-resolution structure of these distinct Aβ42 conformers would require ssNMR or cryo-EM. Nevertheless, the LCOs may provide a new tool for identifying particularly malignant AD cases in a diagnostic neuropathological setting.

In accordance with our earlier report (17), these data showed remarkable intraindividual and interindividual

structural diversity of Aβ in AD, and the rapid disease progression is strongly linked to a distinct subset of Aβ conformers. These recent advances raise a series of critical mechanistic questions regarding the role of pathogenic aggregates of Aβ and tau in distinct phenotypes of sAD and in fAD: (i) What is the high-resolution structural organization of brain-derived Aβ in rapidly and slowly progressive sAD and in fAD? (ii) Which structural features of Aβ control the apparent diversity of the pathological and clinical features in sAD and fAD? (iii) What are the critical interactomes of distinct Aβ strains? As exemplified in one recent study that suggests pathological α-syn may serve as one of the major interactomes causing tau cross-seeding in the transgenic mice with abundant Aβ plaques (67). Addressing these questions is of fundamental importance for advancing the emerging concept that structurally distinct prion-like strains of Aβ are critical differentiating factors in the sAD and fAD development and propagation in the brain. In light of the proposed transmissibility of AD pathology from person to person (68), critically reviewed in the recent white paper (51), these mechanistic questions may have crucial biosafety implications and point to the urgent need for novel methods that can accurately detect and differentiate prion-like forms of Aβ aggregates. The discovery of disease-modifying drugs for AD and fAD is directly related to the progress in diagnostic methods that are able to differentiate and track different strains of Aβ aggregates and thus detect cases with a high risk of rapid progression. New amplification methods now allow the ultrasensitive detection and differentiation of human prion, synuclein, and tau protein strains in cerebrospinal fluid, nasal brushings, and skin (69–72); and such Aβ strain typing could provide a "tracer" in cases of brain trauma that carry a high risk of transition to AD, so preventive measures or therapy can be instituted. The data accumulated in this study may provide a steppingstone for a broader development of novel structure-based diagnostic classification of AD and related proteinopathies.

Experimental procedures

Ethics statement

All procedures were strictly implemented under the standard protocols approved by the Institutional Review Board at schools of medicine, NYU, Case Western Reserve University, and University Hospitals Case Medical Centre. For all the cases associated with our investigation, written informed consents for research were acquired from patients' or legal guardians, and the material during research had appropriate ethical approval for use in this project. All patients' data and samples were coded and operated in accordance with the National Institutes of Health (NIH) guidelines in order to protect patients' identities. The studies abide by the Declaration of Helsinki principles.

Human brain samples

The rpAD cases and 24 non-AD control cases including sporadic Creutzfeldt–Jakob disease were randomly selected from a cohort of a group of patients who were referred to the NPDPSC from 2012 to 2015, with a rapidly progressive dementia and differential diagnosis of prion disease. For all the cases involved in our research, the fAD and sporadic prion diseases were excluded by family history, neuropathology, immunohistochemistry, sequencing of PRNP gene, and molecular typing of PrP^{Sc} by Western blot. To maintain the integrity of this rpAD cohort, other aspects strictly followed the same criteria as in our previous study (17). The spAD cases consisted of those diagnosed at the Alzheimer Disease Clinical Center, Department of Neurology, NYU School of Medicine. These cases under our investigation were confirmed by demographics, descriptive statistics, and classification per NIA-AA Alzheimer's Disease Neuropathologic Change classification, as shown in Table 1.

LCO staining

The synthesis of LCOs (qFTAA and hFTAA) was previously described (27). Brain cryosections (12 μm thick) derived from the brain cortex were thawed at room temperature (RT) for 1 h, fixed in 100% ethanol for 10 min, followed by 70% ethanol for 5 min, subsequently, treated with double-distilled water for 5 min. Next, they were immersed in PBS for 15 min, stained by adding either 1.5 μM hFTAA or qFTAA in PBS dropwise to tissue sections for 30 min at RT, and then rinsed by PBS for 3 × 5 min. They were then allowed to dry under ambient conditions, mounted with the DAKO mounting medium (Sigma–Aldrich; DUO82040), sealed with a nail polish, and settled overnight for further experimental purposes (31).

Fluorescence images and spectral analysis

Cored or diffuse Aβ deposits stained by LCOs were imaged using HC PLAPO C52 40× (1.30 Oil) objective by λ scan mode (with bandwidth of 10 nm and a filter switch) of Confocal Leica SP8 microscope equipped with Argon laser using an excitation wavelength of 458 nm and HyD2 Detector at 1024 × 1024 pixel resolution provided by Light Microscopy Imaging Core at Case Western Reserve University. After the fluorescent images were collected by confocal microscopy, ten regions of interest were selected in each plaque, and the fluorescence spectral profile was recorded by semiautomated Leica LAX software. A minimum of ten emission spectra were recorded with qFTAA and hFTAA in 10 compact (cored) and ten diffuse plaques in frontal, occipital, and temporal cortex of rapidly and spAD phenotype. For each plaque, we utilized ten regions of interests to average the fluorescence emission intensity at each corresponding wavelength ranging from 470 to 690 nm with the bandwidth of 10 nm. The mean fluorescence emission spectra were normalized by peak intensity at 500 nm (for qFTAA) or 550 nm (for hFTAA) with excitation wavelength at 458 nm.

Immunohistochemistry

The AD brain tissues were sectioned in 12 μm thickness and fixed in acetone at −20 °C for 5 min, dried for 30 min, and rehydration in PBS for 1 min. These sections were then

blocked in 5% normal goat serum (Thermo Fisher Scientific; 50062Z) in PBS at RT for 30 min, incubated in a conformational-specific antibody OC (Millipore; AB2286) with dilution 1:1000 in blocking buffer at 4 °C overnight. Next, they were washed with PBS for 3 × 5 min, incubated with the anti-rabbit secondary antibody-conjugated peroxidase or with Alexa Fluor 633 (Invitrogen; A-21070) in blocking buffer (1:200 dilution) at RT for 1 h. The sections were washed with PBS for 3 × 5 min before and after incubated with 1.5 μM q-FTAA or 1.5 μM h-FTAA (62). The sections were then dried under ambient conditions, covered with Duolink mounting medium containing 4′,6-diamidino-2-phenylindole, and sealed with a nail polish. Fluorescence images were acquired using Leica TCS SP8 confocal microscope with HC PL APO CS2 40×/1.30 Oil objective, Pinhole 65.3 μm, and laser sources including 405 diode, 458 argon with 20% power, HeNe 633. In addition, detectors were sequentially set as follows: PMT 3 (640–660 nm), HyD2 (535–558 nm) standard mode, and PMT 1 (419–439 nm).

Double LCO labeling

Cryosections derived from a cohort of patients with rpAD and spAD were stained by a mixture of LCOs (qFTAA and hFTAA) as described (49). In short, a mixture containing 1 μM qFTAA and 0.5 μM hFTAA was applied to the cryosections after fixation and rehydration as described previously. Hyperspectral images were collected the following day using LeicaDM6000B microscope equipped with Spectral cube (Applied Spectral imaging from the Department of Physics, Chemistry and Biology, Linköping University, Sweden) for hyperspectral imaging. Excitation was set at 436 nm, and spectra were collected between 480 and 700 nm using a long pass filter.

Concentration and conformation of Aβ42

The CDI was performed as described previously with minor modifications (17). Briefly, for the detection of Aβ42, we used the donor and acceptor beads coated with mAb 8G4 specific for N terminus (epitope human Aβ residues 17–24) and mAb specific for C terminus of Aβ42 (12F4) (PerkinElmer). The 96-well half-area light gray plates (PerkinElmer) were first filled with 20 μl per well of 12.5 μg/ml of acceptor beads and 1.25 nM biotinylated mAb. Thawed samples were sonicated with three 5 s cycles using Misonix Sonicator 4000 at 80% power output and made into two 4 μl aliquots: native (N) and denatured (D). The native sample was mixed with 28 μl of assay buffer (PerkinElmer) and kept at RT; the second aliquot was denatured with 28 μl of final 7 M GdnHCl at 80 °C for 10 min. Both native and denatured aliquots were diluted with 80 μl of assay buffer, 5 μl loaded immediately onto the plate, and incubated at RT for 2 h. Next, 25 μl of 40 μg/ml of streptavidin-coated donor beads were added per well and incubated 1 h at RT. Fluorescence signals were measured by multimode microplate reader PHERAstar Plus (BMG LabTech) and "AlphaScreen" PHERAstar Plus software. Concentrations of the samples were calculated from the signal of denatured sample and standard dilution curve of Aβ42 peptides and are expressed in nanogram per millimeter of the original 10% (w/v) brain homogenate. The ratio of D/N signal is proportional to the concentration of N-terminal and C-terminal epitopes that are hidden in the native state because of the formation of the polymeric assemblies of misfolded proteins (12, 18, 19, 21).

Statistics

Cumulative survival curves were constructed by the Kaplan–Meier method, both overall and by stratifying for each variable, and comparisons of survival curves among groups were carried out by the log rank (Mantel–Cox) test. The effect of concentration and conformation obtained with CDI in clinicopathological phenotype, and duration of the disease in AD cases was calculated using two-way ANOVA and two-tailed Fisher's exact test. The statistical values for different anatomical regions of rpAD and spAD cases per amyloid plaque morphotype were assessed by multiple *t* tests with Kaleidagraph (Synergy), Prism 8 (GraphPad Software, Inc), and SPSS 27 software (SPSS, Inc).

Data availability

All data generated during the experimental procedures in this article are and/or available based on request.

Supporting information—This article contains supporting information.

Acknowledgments—We are grateful to the patients' families for donating brain tissue. We thank all the referring physicians and members of the NPDPSC, Cleveland, OH, for assistance and review of clinical data. Work in the Safar laboratory was supported by grants from Alberta Innovates Bio Solutions (FP00209618) and NIH (1RF1AG058267 and 1RF1AG061797); work at NYU was supported by NIH grant (1RF1AG061797, AG066512, and AG060882), and the Linköping laboratories were supported by Swedish Research Council (grant nos.: 2019-04405 and 2016-00748), the Swedish Alzheimer Foundation, the Swedish Brain Foundation, and the Torsten Söderberg Foundation.

Author contributions—H. L. and J. G. S. conceptualization; H. L., C. K., T. H., C. J. S., S. N., K. P. R. N., M. L. C., T. W., P. H., and J. G. S. data curation; H. L. writing–original draft; J. G. S. writing–review and editing; J. G. S. supervision; J. G. S. funding acquisition.

Funding and additional information—The content is solely the responsibility of the authors and does not necessarily represent the official views of the NIH.

Conflict of interest—The authors declare that they have no conflicts of interest with the contents of this article.

Abbreviations—The abbreviations used are: Aβ, amyloid beta; Aβ40, human amyloid beta peptide with amino acid sequence 1 to 40; Aβ42, human amyloid beta peptide with amino acid sequence 1 to 42; AD, Alzheimer's disease; *APOE*, apolipoprotein E gene with ε2, ε3, or ε4 allelic polymorphisms; *APP*, amyloid precursor protein gene; CDI, conformation-dependent immunoassay; D/N, denatured/native signal; fAD, familial AD; hFTAA,

heptaformylthiophene acetic acid; GdnHCl, guanidine hydrochloride; LCO, luminescent conjugated oligothiophene; mAb, monoclonal antibody; NFT, neurofibrillary tangle; NIA-AA, National Institutes of Aging—Alzheimer's Association; NIH, the National Institutes of Health; NPDPSC, National Prion Disease Pathology Surveillance Center; NYU, New York University; PRNP, prion protein; qFTAA, quatroformylthiophene acetic acid; rpAD, rapidly progressive AD; RT, room temperature; sAD, sporadic AD; spAD, slowly progressive AD; ssNMR, solid-state NMR.

References

1. Braak, H., and Del Tredici, K. (2013) Evolutional aspects of Alzheimer's disease pathogenesis. *J. Alzheimers Dis.* **33 Suppl 1**, S155–161
2. Murray, M. E., Graff-Radford, N. R., Ross, O. A., Petersen, R. C., Duara, R., and Dickson, D. W. (2011) Neuropathologically defined subtypes of Alzheimer's disease with distinct clinical characteristics: A retrospective study. *Lancet Neurol.* **10**, 785–796
3. Risacher, S. L., Anderson, W. H., Charil, A., Castelluccio, P. F., Shcherbinin, S., Saykin, A. J., and Schwarz, A. J. (2017) Alzheimer disease brain atrophy subtypes are associated with cognition and rate of decline. *Neurology* **89**, 2176–2186
4. Mrdjen, D., Fox, E. J., Bukhari, S. A., Montine, K. S., Bendall, S. C., and Montine, T. J. (2019) The basis of cellular and regional vulnerability in Alzheimer's disease. *Acta Neuropathol.* **138**, 729–749
5. Schellenberg, G. D., and Montine, T. J. (2012) The genetics and neuropathology of Alzheimer's disease. *Acta Neuropathol.* **124**, 305–323
6. Selkoe, D. J. (2011) Alzheimer's disease. *Cold Spring Harb. Perspect. Biol.* **3**
7. Van Cauwenberghe, C., Van Broeckhoven, C., and Sleegers, K. (2016) The genetic landscape of Alzheimer disease: Clinical implications and perspectives. *Genet. Med.* **18**, 421–430
8. Congdon, E. E., and Sigurdsson, E. M. (2018) Tau-targeting therapies for Alzheimer disease. *Nat. Rev. Neurol.* **14**, 399–415
9. Gallardo, G., and Holtzman, D. M. (2019) Amyloid-β and tau at the crossroads of Alzheimer's disease. *Adv. Exp. Med. Biol.* **1184**, 187–203
10. Selkoe, D. J., and Hardy, J. (2016) The amyloid hypothesis of Alzheimer's disease at 25 years. *EMBO Mol. Med.* **8**, 595–608
11. Cohen, M., Appleby, B., and Safar, J. G. (2016) Distinct prion-like strains of amyloid beta implicated in phenotypic diversity of Alzheimer's disease. *Prion* **10**, 9–17
12. Haldiman, T., Kim, C., Cohen, Y., Chen, W., Blevins, J., Qing, L., Cohen, M. L., Langeveld, J., Telling, G. C., Kong, Q., and Safar, J. G. (2013) Coexistence of distinct prion types enables conformational evolution of human PrPSc by competitive selection. *J. Biol. Chem.* **288**, 29846–29861
13. Meyer-Luehmann, M., Coomaraswamy, J., Bolmont, T., Kaeser, S., Schaefer, C., Kilger, E., Neuenschwander, A., Abramowski, D., Frey, P., Jaton, A. L., Vigouret, J. M., Paganetti, P., Walsh, D. M., Mathews, P. M., Ghiso, J., *et al.* (2006) Exogenous induction of cerebral beta-amyloidogenesis is governed by agent and host. *Science* **313**, 1781–1784
14. Prusiner, S. B. (2012) Cell biology. A unifying role for prions in neurodegenerative diseases. *Science* **336**, 1511–1513
15. Prusiner, S. B. (2013) Biology and genetics of prions causing neurodegeneration. *Annu. Rev. Genet.* **47**, 601–623
16. Safar, J. G. (2012) Molecular pathogenesis of sporadic prion diseases in man. *Prion* **6**, 108–115
17. Cohen, M. L., Kim, C., Haldiman, T., ElHag, M., Mehndiratta, P., Pichet, T., Lissemore, F., Shea, M., Cohen, Y., Chen, W., Blevins, J., Appleby, B. S., Surewicz, K., Surewicz, W. K., Sajatovic, M., *et al.* (2015) Rapidly progressive Alzheimer's disease features distinct structures of amyloid-β. *Brain* **138**, 1009–1022
18. Kim, C., Haldiman, T., Cohen, Y., Chen, W., Blevins, J., Sy, M. S., Cohen, M., and Safar, J. G. (2011) Protease-sensitive conformers in broad spectrum of distinct PrPSc structures in sporadic Creutzfeldt-Jakob disease are indicator of progression rate. *PLoS Pathog.* **7**, e1002242
19. Kim, C., Haldiman, T., Surewicz, K., Cohen, Y., Chen, W., Blevins, J., Sy, M. S., Cohen, M., Kong, Q., Telling, G. C., Surewicz, W. K., and Safar, J. G. (2012) Small protease sensitive oligomers of PrPSc in distinct human prions determine conversion rate of PrP(C). *PLoS Pathog.* **8**, e1002835
20. Kim, C., Xiao, X., Chen, S., Haldiman, T., Smirnovas, V., Kofskey, D., Warren, M., Surewicz, K., Maurer, N. R., Kong, Q., Surewicz, W., and Safar, J. G. (2018) Artificial strain of human prions created *in vitro*. *Nat. Commun.* **9**, 2166
21. Safar, J., Wille, H., Itri, V., Groth, D., Serban, H., Torchia, M., Cohen, F. E., and Prusiner, S. B. (1998) Eight prion strains have PrP(Sc) molecules with different conformations. *Nat. Med.* **4**, 1157–1165
22. Qiang, W., Yau, W. M., Lu, J. X., Collinge, J., and Tycko, R. (2017) Structural variation in amyloid-β fibrils from Alzheimer's disease clinical subtypes. *Nature* **541**, 217–221
23. Liu, J., Costantino, I., Venugopalan, N., Fischetti, R. F., Hyman, B. T., Frosch, M. P., Gomez-Isla, T., and Makowski, L. (2016) Amyloid structure exhibits polymorphism on multiple length scales in human brain tissue. *Sci. Rep.* **6**, 33079
24. Kollmer, M., Close, W., Funk, L., Rasmussen, J., Bsoul, A., Schierhorn, A., Schmidt, M., Sigurdson, C. J., Jucker, M., and Fändrich, M. (2019) Cryo-EM structure and polymorphism of Aβ amyloid fibrils purified from Alzheimer's brain tissue. *Nat. Commun.* **10**, 4760
25. Aslund, A., Sigurdson, C. J., Klingstedt, T., Grathwohl, S., Bolmont, T., Dickstein, D. L., Glimsdal, E., Prokop, S., Lindgren, M., Konradsson, P., Holtzman, D. M., Hof, P. R., Heppner, F. L., Gandy, S., Jucker, M., *et al.* (2009) Novel pentameric thiophene derivatives for *in vitro* and *in vivo* optical imaging of a plethora of protein aggregates in cerebral amyloidoses. *ACS Chem. Biol.* **4**, 673–684
26. Herrmann, U. S., Schütz, A. K., Shirani, H., Huang, D., Saban, D., Nuvolone, M., Li, B., Ballmer, B., Åslund, A. K., Mason, J. J., Rushing, E., Budka, H., Nyström, S., Hammarström, P., Böckmann, A., *et al.* (2015) Structure-based drug design identifies polythiophenes as antiprion compounds. *Sci. Transl. Med.* **7**, 299ra123
27. Klingstedt, T., Aslund, A., Simon, R. A., Johansson, L. B., Mason, J. J., Nyström, S., Hammarström, P., and Nilsson, K. P. (2011) Synthesis of a library of oligothiophenes and their utilization as fluorescent ligands for spectral assignment of protein aggregates. *Org. Biomol. Chem.* **9**, 8356–8370
28. Klingstedt, T., Blechschmidt, C., Nogalska, A., Prokop, S., Häggqvist, B., Danielsson, O., Engel, W. K., Askanas, V., Heppner, F. L., and Nilsson, K. P. (2013) Luminescent conjugated oligothiophenes for sensitive fluorescent assignment of protein inclusion bodies. *Chembiochem* **14**, 607–616
29. Klingstedt, T., and Nilsson, K. P. (2012) Luminescent conjugated poly- and oligo-thiophenes: Optical ligands for spectral assignment of a plethora of protein aggregates. *Biochem. Soc. Trans.* **40**, 704–710
30. Klingstedt, T., Shirani, H., Åslund, K. O., Cairns, N. J., Sigurdson, C. J., Goedert, M., and Nilsson, K. P. (2013) The structural basis for optimal performance of oligothiophene-based fluorescent amyloid ligands: Conformational flexibility is essential for spectral assignment of a diversity of protein aggregates. *Chemistry* **19**, 10179–10192
31. Nyström, S., Bäck, M., Nilsson, K. P. R., and Hammarström, P. (2017) Imaging amyloid tissues stained with luminescent conjugated oligothiophenes by hyperspectral confocal microscopy and fluorescence lifetime imaging. *J. Vis. Exp.*, 56279
32. Rasmussen, J., Mahler, J., Beschorner, N., Kaeser, S. A., Häsler, L. M., Baumann, F., Nyström, S., Portelius, E., Blennow, K., Lashley, T., Fox, N. C., Sepulveda-Falla, D., Glatzel, M., Oblak, A. L., Ghetti, B., *et al.* (2017) Amyloid polymorphisms constitute distinct clouds of conformational variants in different etiological subtypes of Alzheimer's disease. *Proc. Natl. Acad. Sci. U. S. A.* **114**, 13018–13023
33. Aguilar-Calvo, P., Sevillano, A. M., Bapat, J., Soldau, K., Sandoval, D. R., Altmeppen, H. C., Linsenmeier, L., Pizzo, D. P., Geschwind, M. D., Sanchez, H., Appleby, B. S., Cohen, M. L., Safar, J. G., Edland, S. D., Glatzel, M., *et al.* (2020) Shortening heparan sulfate chains prolongs survival and reduces parenchymal plaques in prion disease caused by mobile, ADAM10-cleaved prions. *Acta Neuropathol.* **139**, 527–546
34. Magnusson, K., Simon, R., Sjölander, D., Sigurdson, C. J., Hammarström, P., and Nilsson, K. P. (2014) Multimodal fluorescence microscopy of

prion strain specific PrP deposits stained by thiophene-based amyloid ligands. *Prion* **8**, 319–329
35. Sigurdson, C. J., Nilsson, K. P., Hornemann, S., Manco, G., Polymenidou, M., Schwarz, P., Leclerc, M., Hammarström, P., Wüthrich, K., and Aguzzi, A. (2007) Prion strain discrimination using luminescent conjugated polymers. *Nat. Methods* **4**, 1023–1030
36. Lau, H. H. C., Ingelsson, M., and Watts, J. C. (2021) The existence of Aβ strains and their potential for driving phenotypic heterogeneity in Alzheimer's disease. *Acta Neuropathol.* **142**, 17–39
37. Pillai, J. A., Appleby, B. S., Safar, J., and Leverenz, J. B. (2018) Rapidly progressive Alzheimer's disease in two distinct autopsy cohorts. *J. Alzheimers Dis.* **64**, 973–980
38. Pillai, J. A., Bonner-Jackson, A., Bekris, L. M., Safar, J., Bena, J., and Leverenz, J. B. (2019) Highly elevated cerebrospinal fluid total tau level reflects higher likelihood of non-amnestic subtype of Alzheimer's disease. *J. Alzheimers Dis.* **70**, 1051–1058
39. Schmidt, C., Wolff, M., Weitz, M., Bartlau, T., Korth, C., and Zerr, I. (2011) Rapidly progressive Alzheimer disease. *Arch. Neurol.* **68**, 1124–1130
40. Akiyama, H., Mori, H., Saido, T., Kondo, H., Ikeda, K., and McGeer, P. L. (1999) Occurrence of the diffuse amyloid beta-protein (Abeta) deposits with numerous Abeta-containing glial cells in the cerebral cortex of patients with Alzheimer's disease. *Glia* **25**, 324–331
41. Schmidt, C., Karch, A., Artjomova, S., Hoeschel, M., and Zerr, I. (2013) Pre-progression rates in Alzheimer's disease revisited. *J. Alzheimers Dis.* **35**, 451–454
42. Schmidt, C., Redyk, K., Meissner, B., Krack, L., von Ahsen, N., Roeber, S., Kretzschmar, H., and Zerr, I. (2010) Clinical features of rapidly progressive Alzheimer's disease. *Dement Geriatr. Cogn. Disord.* **29**, 371–378
43. Schmidt, C., Wolff, M., von Ahsen, N., and Zerr, I. (2012) Alzheimer's disease: Genetic polymorphisms and rate of decline. *Dement Geriatr. Cogn. Disord.* **33**, 84–89
44. Prusiner, S. B. (2004). In: Prusiner, S. B., ed. *Prion Biology and Diseases*, 2nd Ed., Cold Spring Harbor Laboratory Press, Cold Spring Harbor, NY
45. Safar, J. G. (2013) Molecular mechanisms encoding quantitative and qualitative traits of prion strains. In: Zou, W.-Q., Gambetti, P., eds. *Prions and Diseases: Volume 1, Physiology and Pathophysiology*, Springer New York, New York, NY: 161–179
46. Safar, J. G., Scott, M., Monaghan, J., Deering, C., Didorenko, S., Vergara, J., Ball, H., Legname, G., Leclerc, E., Solforosi, L., Serban, H., Groth, D., Burton, D. R., Prusiner, S. B., and Williamson, R. A. (2002) Measuring prions causing bovine spongiform encephalopathy or chronic wasting disease by immunoassays and transgenic mice. *Nat. Biotechnol.* **20**, 1147–1150
47. Hammarström, P. (2019) Photonic amyloids. *Nat. Photon.* **13**, 442–444
48. Masters, C. L., and Selkoe, D. J. (2012) Biochemistry of amyloid β-protein and amyloid deposits in Alzheimer disease. *Cold Spring Harb. Perspect. Med.* **2**, a006262
49. Nyström, S., Psonka-Antonczyk, K. M., Ellingsen, P. G., Johansson, L. B., Reitan, N., Handrick, S., Prokop, S., Heppner, F. L., Wegenast-Braun, B. M., Jucker, M., Lindgren, M., Stokke, B. T., Hammarström, P., and Nilsson, K. P. (2013) Evidence for age-dependent *in vivo* conformational rearrangement within Aβ amyloid deposits. *ACS Chem. Biol.* **8**, 1128–1133
50. Nelson, P. T., Alafuzoff, I., Bigio, E. H., Bouras, C., Braak, H., Cairns, N. J., Castellani, R. J., Crain, B. J., Davies, P., Del Tredici, K., Duyckaerts, C., Frosch, M. P., Haroutunian, V., Hof, P. R., Hulette, C. M., *et al.* (2012) Correlation of Alzheimer disease neuropathologic changes with cognitive status: A review of the literature. *J. Neuropathol. Exp. Neurol.* **71**, 362–381
51. Asher, D. M., Belay, E., Bigio, E., Brandner, S., Brubaker, S. A., Caughey, B., Clark, B., Damon, I., Diamond, M., Freund, M., Hyman, B. T., Jucker, M., Keene, C. D., Lieberman, A. P., Mackiewicz, M., *et al.* (2020) Risk of transmissibility from neurodegenerative disease-associated proteins: Experimental knowns and unknowns. *J. Neuropathol. Exp. Neurol.* **79**, 1141–1146
52. Braak, H., and Braak, E. (1995) Staging of Alzheimer's disease-related neurofibrillary changes. *Neurobiol. Aging* **16**, 271–278. discussion 278-284
53. Guo, J. L., and Lee, V. M. (2014) Cell-to-cell transmission of pathogenic proteins in neurodegenerative diseases. *Nat. Med.* **20**, 130–138
54. Ringman, J. M., Goate, A., Masters, C. L., Cairns, N. J., Danek, A., Graff-Radford, N., Ghetti, B., and Morris, J. C. (2014) Genetic heterogeneity in Alzheimer disease and implications for treatment strategies. *Curr. Neurol. Neurosci. Rep.* **14**, 499
55. Shinohara, M., Fujioka, S., Murray, M. E., Wojtas, A., Baker, M., Rovelet-Lecrux, A., Rademakers, R., Das, P., Parisi, J. E., Graff-Radford, N. R., Petersen, R. C., Dickson, D. W., and Bu, G. (2014) Regional distribution of synaptic markers and APP correlate with distinct clinicopathological features in sporadic and familial Alzheimer's disease. *Brain* **137**, 1533–1549
56. Tabira, T., Chui, D. H., and Kuroda, S. (2002) Significance of intracellular Abeta42 accumulation in Alzheimer's disease. *Front. Biosci.* **7**, a44–49
57. Kabir, M. E., and Safar, J. G. (2014) Implications of prion adaptation and evolution paradigm for human neurodegenerative diseases. *Prion* **8**, 111–116
58. Xiao, Y., Ma, B., McElheny, D., Parthasarathy, S., Long, F., Hoshi, M., Nussinov, R., and Ishii, Y. (2015) Aβ(1-42) fibril structure illuminates self-recognition and replication of amyloid in Alzheimer's disease. *Nat. Struct. Mol. Biol.* **22**, 499–505
59. Daebel, V., Chinnathambi, S., Biernat, J., Schwalbe, M., Habenstein, B., Loquet, A., Akoury, E., Tepper, K., Müller, H., Baldus, M., Griesinger, C., Zweckstetter, M., Mandelkow, E., Vijayan, V., and Lange, A. (2012) β-Sheet core of tau paired helical filaments revealed by solid-state NMR. *J. Am. Chem. Soc.* **134**, 13982–13989
60. Fitzpatrick, A. W. P., Falcon, B., He, S., Murzin, A. G., Murshudov, G., Garringer, H. J., Crowther, R. A., Ghetti, B., Goedert, M., and Scheres, S. H. W. (2017) Cryo-EM structures of tau filaments from Alzheimer's disease. *Nature* **547**, 185–190
61. Gremer, L., Schölzel, D., Schenk, C., Reinartz, E., Labahn, J., Ravelli, R. B. G., Tusche, M., Lopez-Iglesias, C., Hoyer, W., Heise, H., Willbold, D., and Schröder, G. F. (2017) Fibril structure of amyloid-β(1-42) by cryo-electron microscopy. *Science* **358**, 116–119
62. Klingstedt, T., Ghetti, B., Holton, J. L., Ling, H., Nilsson, K. P. R., and Goedert, M. (2019) Luminescent conjugated oligothiophenes distinguish between α-synuclein assemblies of Parkinson's disease and multiple system atrophy. *Acta Neuropathol. Commun.* **7**, 193
63. Arppe, R., Carro-Temboury, M. R., Hempel, C., Vosch, T., and Just Sørensen, T. (2017) Investigating dye performance and crosstalk in fluorescence enabled bioimaging using a model system. *PLoS One* **12**, e0188359
64. Drummond, E., Nayak, S., Faustin, A., Pires, G., Hickman, R. A., Askenazi, M., Cohen, M., Haldiman, T., Kim, C., Han, X., Shao, Y., Safar, J. G., Ueberheide, B., and Wisniewski, T. (2017) Proteomic differences in amyloid plaques in rapidly progressive and sporadic Alzheimer's disease. *Acta Neuropathol.* **133**, 933–954
65. Michno, W., Nyström, S., Wehrli, P., Lashley, T., Brinkmalm, G., Guerard, L., Syvänen, S., Sehlin, D., Kaya, I., Brinet, D., Nilsson, K. P. R., Hammarström, P., Blennow, K., Zetterberg, H., and Hanrieder, J. (2019) Pyroglutamation of amyloid-βx-42 (Aβx-42) followed by Aβ1-40 deposition underlies plaque polymorphism in progressing Alzheimer's disease pathology. *J. Biol. Chem.* **294**, 6719–6732
66. Mori, H., Takio, K., Ogawara, M., and Selkoe, D. J. (1992) Mass spectrometry of purified amyloid beta protein in Alzheimer's disease. *J. Biol. Chem.* **267**, 17082–17086
67. Bassil, F., Brown, H. J., Pattabhiraman, S., Iwasyk, J. E., Maghames, C. M., Meymand, E. S., Cox, T. O., Riddle, D. M., Zhang, B., Trojanowski, J. Q., and Lee, V. M. (2020) Amyloid-beta (Aβ) plaques promote seeding and spreading of alpha-synuclein and tau in a mouse model of lewy body disorders with Aβ pathology. *Neuron* **105**, 260–275.e266
68. Jaunmuktane, Z., Mead, S., Ellis, M., Wadsworth, J. D., Nicoll, A. J., Kenny, J., Launchbury, F., Linehan, J., Richard-Loendt, A., Walker, A. S., Rudge, P., Collinge, J., and Brandner, S. (2015) Evidence for human transmission of amyloid-β pathology and cerebral amyloid angiopathy. *Nature* **525**, 247–250
69. Foutz, A., Appleby, B. S., Hamlin, C., Liu, X., Yang, S., Cohen, Y., Chen, W., Blevins, J., Fausett, C., Wang, H., Gambetti, P., Zhang, S., Hughson,

A., Tatsuoka, C., Schonberger, L. B., *et al.* (2017) Diagnostic and prognostic value of human prion detection in cerebrospinal fluid. *Ann. Neurol.* **81**, 79–92

70. Groveman, B. R., Orrù, C. D., Hughson, A. G., Raymond, L. D., Zanusso, G., Ghetti, B., Campbell, K. J., Safar, J., Galasko, D., and Caughey, B. (2018) Rapid and ultra-sensitive quantitation of disease-associated α-synuclein seeds in brain and cerebrospinal fluid by αSyn RT-QuIC. *Acta Neuropathol. Commun.* **6**, 7
71. Metrick, M. A., 2nd, Ferreira, N. D. C., Saijo, E., Kraus, A., Newell, K., Zanusso, G., Vendruscolo, M., Ghetti, B., and Caughey, B. (2020) A single ultrasensitive assay for detection and discrimination of tau aggregates of Alzheimer and Pick diseases. *Acta Neuropathol. Commun.* **8**, 22
72. Orrú, C. D., Yuan, J., Appleby, B. S., Li, B., Li, Y., Winner, D., Wang, Z., Zhan, Y. A., Rodgers, M., Rarick, J., Wyza, R. E., Joshi, T., Wang, G. X., Cohen, M. L., Zhang, S., *et al.* (2017) Prion seeding activity and infectivity in skin samples from patients with sporadic Creutzfeldt-Jakob disease. *Sci. Transl. Med.* **9**, eaam7785
73. Montine, T. J., Phelps, C. H., Beach, T. G., Bigio, E. H., Cairns, N. J., Dickson, D. W., Duyckaerts, C., Frosch, M. P., Masliah, E., Mirra, S. S., Nelson, P. T., Schneider, J. A., Thal, D. R., Trojanowski, J. Q., Vinters, H. V., *et al.* (2012) National Institute on aging-Alzheimer's association guidelines for the neuropathologic assessment of Alzheimer's disease: A practical approach. *Acta Neuropathol.* **123**, 1–11